Heat and mass transfer during the violent collapse of nonspherical bubbles

Andrew J. Szeri
Department of Mechanical Engineering, University of California, Berkeley, California 94720-1740

Brian D. Storey
Franklin W. Olin College of Engineering, 1795 Great Plain Avenue, Needham, Massachusetts 02492-1245

Antony Pearson and John R. Blake
School of Mathematics and Statistics, The University of Birmingham, Edgbaston, Birmingham B15 2TT, United Kingdom

(Received 15 November 2002; accepted 5 June 2003; published 1 August 2003)

The very high speed of collapse of cavitation bubbles is responsible for a number of phenomena of interest in science and engineering: Luminescence, sonochemistry, cavitation damage, ultrasonic cleaning, etc. Strongly forced bubbles may collapse with such violence that the relatively slow processes of diffusion of the heat of compression and of excess vapor to the bubble wall are obviated. This leads to an approximately adiabatic system with nearly constant mass during the final stages of extreme collapses, accompanied by the evolution of sharp thermal and compositional boundary layers on either side of the interface. It is shown that the boundary layers, which are involved in the determination of the interfacial temperature through the balance of sensible and latent heats, may profitably be described mathematically through integral equations. This complements well the boundary integral solution of the fluid dynamics, which has been the basis of much progress in the field. © *2003 American Institute of Physics.* [DOI: 10.1063/1.1595647]

I. INTRODUCTION

When a bubble collapses near another bubble, a wall, free surface, in a static or dynamic pressure gradient and in other situations, it may suffer from an instability that drives the shape to be nonspherical.[1] The collapsing nonspherical bubble may develop a strong jet which is associated with cavitation damage on a wall.[2] As an illustration, in a bubble field employed for the purposes of sonochemistry, nonspherical bubble collapse is associated with the acoustic pressure field, acoustic streaming and nearby bubbles. This changes the features of the collapse important to sonochemistry, such as peak temperatures, pressures, strain rates, mixing, and radical production. The collapses can be sufficiently violent that luminescence is produced.[3,4]

In many applications heat and mass transfer to and from the bubble are of importance. In the case of cavitation damage at a wall, the amount of gas that flows into the growing bubble during expansion will determine what quantity of noncondensible remnants will provide new nuclei for the next event. In sonochemistry, the transport of vapor into the interior, and the flow (of some) of the heat of compression out into the liquid are crucial physical processes to include in a model to determine free radical production.

Heat and mass transfer in nonspherical bubble collapse have been the subject of inquiry by numerical methods before. Yuan and Prosperetti[5] attached a moving grid in the gas to the bubble wall, in order to solve transport equations by finite differences and determine the thermal boundary layer structure. Yasuda and Takahira[6] have used an unstructured grid to solve by finite volumes the transport equations in the bubble interior. Both groups used the boundary integral technique to account for the (irrotational) fluid motion outside the bubble. Both report difficulties in resolving the very thin boundary layers near the interfaces of violently collapsing bubbles. Neither group considered mass transfer or the thermal boundary layer in the liquid.

In the present work, we also begin with a boundary integral simulation of the nonspherical collapse of a bubble developed by Blake *et al.*[7–10] We develop an integral equation form of the balance of sensible and latent heats at the interface that accounts for heat and mass transfer in the boundary layers within and outside of the bubble. The method we develop rests on one basic fact: That a material filament in the fluid normal to a shear-free interface at one instant, stays forever normal to that interface.[11] Such a material filament, or more precisely such a filament at the place where it meets the surface, is the back-bone on which our method is constructed. Such surface-normal filaments have been used before in order to account for the effects of viscosity.[12,13]

When there are boundary layers, we make two assumptions (beyond the shear-free interface) to enable solution of the transport problem. The first is that the boundary layers are thin. The second is that surface-normal gradients dominate surface parallel gradients. We make use of these assumptions to write convective-diffusive transport equations along the surface-normal material filament. These are partial differential equations in the normal direction and time. There is no convective term as the filament is a material filament and we work in Lagrangian surface-normal coordinates. There are no diffusive fluxes in the surface parallel direction because by assumption these fluxes are much smaller than surface-normal fluxes.

The assumption that surface-normal gradients (of temperature, vapor fraction, etc.) dominate surface-parallel gradients must be regarded critically. At regions of the surface characterized by high local curvature, one may expect that the assumption is less accurate than over parts of the surface where local curvature is relatively smaller. However, the focus of the present work is on accurate characterization of bulk conditions within the bubble. Regions of the surface where the curvature is high are, of necessity, of limited spatial extent. Moreover the surface-parallel strain is normally not large where the curvature is high, which implies that the normal derivatives (and hence flux per unit area) is correspondingly diminished. Hence, regions of intense curvature contribute little to the net fluxes over the entire bubble surface. The relatively large areas of extensive surface-parallel strain and relaxed curvature have associated with them steep normal gradients which dominate the net flux contributions on which the present work rests.

Similar arguments apply to the assumption of a shear-free interface between gas and liquid. Of course, there is in the physical problem a balance of shear stresses on the gas and liquid sides of the interface. However, because the velocities (and velocity derivatives) in the gas and liquid are driven by the motions of the (same) boundary, and because gas viscosities are much smaller than liquid viscosities, the shear-free condition at the boundary can be expected to hold to a reasonable degree of approximation.[11,13] There is still a generation of vorticity at the boundary,[5,13] which is neglected in the present work, and which leads to a nonzero normal gradient of tangential velocity at the surface.[13] This will cause material filaments to lean from normal at the interface. The question is, what errors are associated with the neglect of this effect? The answer lies in a consideration of the relative magnitude of surface-normal gradients versus surface-parallel gradients at the interface. The fact that material filaments, which we approximate as surface-normal, are tilted by the presence of vorticity near the interface is of consequence only if surface-parallel gradients are of similar magnitude to surface-normal gradients—i.e., at areas of intense curvature. As we have argued these areas are of very limited extent. The net effect of the neglect of vorticity will be small on the net flux of interest in the present work.

These surface-normal filament transport equations can be transformed into canonical linear parabolic partial differential equations (PDEs) by working in the reference configuration in a surface-normal Lagrangian boundary layer coordinate and by re-scaling time as in Ref. 14. The consequence is that the surface-normal filament transport equations are analytically tractable. From the solutions, we can construct terms required for the satisfaction of a balance of sensible and latent heats which must hold at every location on the interface.

In Sec. II we develop the model, which begins with a description of the mixture properties, followed by a discussion of how the mechanics and thermodynamics are coupled through the bubble internal pressure. This is followed by a discussion of how the heat and mass transfer are coupled through the balance of sensible and latent heats at all points on the interface in Sec. III. We give details regarding the computation of boundary layer quantities, and of the method of numerical solution of the governing equations. In Sec. IV we consider examples of violent nonspherical collapses of gas–vapor bubbles to illustrate the capabilities of the model. Special attention is paid to the influences on the peak temperatures achieved in bubbles collapsing in close proximity to one another, or to a wall.

II. FORMULATION OF THE HEAT AND MASS TRANSFER PROBLEM

In a simple model of heat and mass transfer, we consider a bubble whose contents include an ideal gas plus vapor. In general, there are a number of species *i*. The contents of the bubble (gas plus vapor) are assumed to be at uniform pressure, composition and temperature, except for boundary layers in composition and temperature that arise during periods of rapid dynamics. The bubble exchanges heat and mass with the surrounding liquid at a rate that can be determined from an application of the first law of thermodynamics, together with solution of convective-diffusive transport equations for heat and mass.

A. Mixture properties and equation of state

The contents of the bubble are modeled as a simple mixture, with the subscript i used to denote the properties of species i. The mole fraction of species i is x_i; the mass fraction is ω_i. The molar density is $\tilde{n}_i$ and the mass density is $\tilde{\rho}_i$. We indicate dimensional quantities with a tilde. Among these are the mean molecular mass $\tilde{M}=\Sigma_i x_i \tilde{M}_i$, the gas constant for the mixture $\tilde{R}_{\mathrm{mix}}=\Sigma_i \omega_i \overline{R}/\tilde{M}_i$, and the specific heat per unit mass of the mixture $\tilde{c}_{p,\mathrm{mix}}=\Sigma_i \omega_i \tilde{c}_{p,i}$. These are constructed from the molecular mass and specific heat of species i ($\tilde{M}_i$ and $\tilde{c}_{p,i}$, respectively) and the universal gas constant $\overline{R}$. For an ideal gas, $\tilde{R}_{\mathrm{mix}}=\tilde{c}_{p,\mathrm{mix}}-\tilde{c}_{v,\mathrm{mix}}$. The equation of state is simply

$$\tilde{T}_g(\tilde{t})=\frac{\tilde{p}(\tilde{t})\tilde{V}(\tilde{t})}{\overline{R}\Sigma_i \tilde{N}_i(t)}. \tag{1}$$

Here, the number of moles of species i is $\tilde{N}_i$; the pressure is $\tilde{p}$; the volume is $\tilde{V}$; and the temperature is $\tilde{T}_g$. The transport properties of the mixture are determined in the same way as in Ref. 15.

B. Evolution equations for the pressure and composition

The heat and mass transfer have an effect on the fluid dynamics outside the bubble through their modification of the pressure evolution inside the bubble. Therefore, it is of central importance to develop an equation for the evolution of the pressure, which will couple the mechanics and thermodynamics.

We begin with Eq. 18.3–6 of Bird, Stewart, and Lightfoot,[16] applied to the gas–vapor mixture within the bubble

$$\frac{\partial}{\partial \tilde{t}}(\tilde{\rho}\tilde{u}) = -\tilde{\nabla}\cdot[\tilde{\rho}\tilde{u}\tilde{\mathbf{v}} + \tilde{\mathbf{q}} + \tilde{p}\tilde{\mathbf{v}}]. \tag{2}$$

Here the internal energy per unit mass of the mixture is $\tilde{u}$, and the energy flux relative to the mass average velocity $\tilde{\mathbf{v}}$ is $\tilde{\mathbf{q}} \equiv -\tilde{k}_g \tilde{\nabla}\tilde{T}_g + \Sigma_i \overline{H}_i \tilde{\mathbf{J}}_i$. Note that this includes the energy flux caused by inter-diffusion in a mixture of species. $\tilde{k}_g$ is the thermal conductivity of the gas, $\overline{H}_i$ is the partial molal enthalpy of the ith species, and the molar flux relative to the mass average velocity is $\tilde{\mathbf{J}}_i$. In (2), we have neglected gravitational effects, heating due to viscous dissipation and the kinetic energy of the gas.

We integrate over the volume of the bubble $\tilde{V}(\tilde{t})$ [with surface $\partial\tilde{V}(\tilde{t})$] and use the divergence theorem to obtain

$$\int_{\tilde{V}(\tilde{t})} \frac{\partial}{\partial \tilde{t}}(\tilde{\rho}\tilde{u})\mathrm{d}\tilde{V} = -\int_{\partial\tilde{V}(\tilde{t})} \mathbf{e}_n \cdot \left[\tilde{\rho}\tilde{u}\tilde{\mathbf{v}} - \tilde{k}_g\tilde{\nabla}\tilde{T}_g + \sum_i \overline{H}\tilde{\mathbf{J}}_i + \tilde{p}\tilde{\mathbf{v}}\right]\mathrm{d}\tilde{A}.$$

Here $\mathbf{e}_n$ is the unit normal directed toward the interior. Next we add a flux term $\int_{\partial\tilde{V}(\tilde{t})} \mathbf{e}_n \cdot [\tilde{\rho}\tilde{u}\tilde{\mathbf{v}}_l]\mathrm{d}\tilde{A}$ to both sides and use the transport theorem to develop the more convenient form

$$\frac{\mathrm{d}}{\mathrm{d}\tilde{t}}\int_{\tilde{V}(\tilde{t})} \tilde{\rho}\tilde{u}\mathrm{d}\tilde{V} = \int_{\partial\tilde{V}(\tilde{t})} \tilde{k}_g \frac{\partial \tilde{T}_g}{\partial \tilde{n}}\mathrm{d}\tilde{A} - \int_{\partial\tilde{V}(\tilde{t})} \mathbf{e}_n \cdot [\tilde{p}\tilde{\mathbf{v}}_l]\mathrm{d}\tilde{A} - \int_{\partial\tilde{V}(\tilde{t})} \mathbf{e}_n \cdot \left[\sum_i \overline{H}_i \tilde{n}_i \tilde{\mathbf{v}}_{\mathrm{rel}}^{(i)}\right]\mathrm{d}\tilde{A}.$$

The coordinate $\tilde{n}$ is in the normal direction. Here, we have defined $\tilde{\mathbf{v}}_{\mathrm{rel}}^{(i)} \equiv \tilde{\mathbf{v}}_i - \tilde{\mathbf{v}}_l$ as the velocity of species i relative to the moving interface (liquid velocity) $\tilde{\mathbf{v}}_l$. Next we write the left hand side using the definition of enthalpy per unit mass: $\tilde{h} \equiv \tilde{u} + \tilde{p}/\tilde{\rho}$. We also assume uniform pressure and temperature (except at the surface) to obtain

$$\frac{\mathrm{d}\tilde{H}_{\mathrm{tot}}}{\mathrm{d}\tilde{t}} = \frac{\mathrm{d}\tilde{p}}{\mathrm{d}\tilde{t}}\tilde{V} + \int_{\partial\tilde{V}(\tilde{t})} \tilde{k}_g \frac{\partial \tilde{T}_g}{\partial \tilde{n}}\mathrm{d}\tilde{A} - \int_{\partial\tilde{V}(\tilde{t})} \mathbf{e}_n \cdot \left[\sum_i \overline{H}_i \tilde{n}_i \tilde{\mathbf{v}}_{\mathrm{rel}}^{(i)}\right]\mathrm{d}\tilde{A}. \tag{3}$$

Now from the definition $\tilde{H}_{\mathrm{tot}} \equiv \Sigma_i \tilde{N}_i \overline{H}_i$, we use the continuity equation for species i and the equation of state of compute directly

$$\frac{\mathrm{d}\tilde{H}_{\mathrm{tot}}}{\mathrm{d}\tilde{t}} = \tilde{V}\sum_i \overline{H}_i \tilde{R}_i - \int_{\partial\tilde{V}(\tilde{t})} \mathbf{e}_n \cdot \left[\sum_i \overline{H}_i \tilde{n}_i \tilde{\mathbf{v}}_{\mathrm{rel}}^{(i)}\right]\mathrm{d}\tilde{A} + \frac{\gamma}{\gamma-1}\tilde{V}\frac{\mathrm{d}\tilde{p}}{\mathrm{d}\tilde{t}} + \frac{\gamma}{\gamma-1}\tilde{p}\frac{\mathrm{d}\tilde{V}}{\mathrm{d}\tilde{t}} - \frac{\gamma\overline{R}\tilde{T}_g}{\gamma-1}\frac{\mathrm{d}\tilde{N}}{\mathrm{d}\tilde{t}}. \tag{4}$$

$\tilde{R}_i$ is the rate of production through chemical reactions. Next we substitute (4) into (3). Upon rearrangement, and after substitution of the definition of the ratio of specific heats γ of the mixture, this yields

$$\frac{\mathrm{d}\tilde{p}}{\mathrm{d}\tilde{t}} = -\frac{\gamma\tilde{p}}{\tilde{V}}\frac{\mathrm{d}\tilde{V}}{\mathrm{d}\tilde{t}} + \frac{\gamma\tilde{p}}{\tilde{N}}\frac{\mathrm{d}\tilde{N}}{\mathrm{d}\tilde{t}} + \frac{\gamma-1}{\tilde{V}}\int_{\partial\tilde{V}(\tilde{t})} \tilde{k}_g \frac{\partial\tilde{T}_g}{\partial\tilde{n}}\mathrm{d}\tilde{A} - (\gamma-1)\sum_i \overline{H}_i\tilde{R}_i. \tag{5}$$

The number of moles of the different species in the bubble evolves according to the molar flux at the interface and the rate of production by chemical reactions in the uniform interior. Hence, we write

$$\frac{\mathrm{d}\tilde{N}_i}{\mathrm{d}\tilde{t}} = \int_{\partial\tilde{V}(\tilde{t})} \tilde{n}_i \tilde{v}_{n,\mathrm{rel}}^{(i)}\mathrm{d}\tilde{A} + \tilde{R}_i\tilde{V}. \tag{6}$$

Note $\tilde{n}_i = \tilde{\rho}_i/\tilde{M}_i$. Once the pressure and number of moles are known, the temperature of the bubble contents is found from the equation of state.

C. Energy balance at the interface

Finally, all that is required is to connect the heat and mass transfer. The interface is incapable of storing energy, so the heat fluxes must balance to zero there. The balance of sensible and latent heat fluxes at the interface is

$$-\tilde{k}_l\frac{\partial\tilde{T}_l}{\partial\tilde{n}} = \sum_i \tilde{\rho}_i\tilde{v}_{n,\mathrm{rel}}^{(i)}\tilde{h}_{lv}^{(i)} - \tilde{k}_g\frac{\partial\tilde{T}_g}{\partial\tilde{n}}. \tag{7}$$

Of course, (7) should be satisfied point-wise on the surface. The expression for the rate of evaporation or condensation of species i is given by[17]

$$\tilde{\rho}_i\tilde{v}_{n,\mathrm{rel}}^{(i)} = -\sigma\sqrt{\frac{\tilde{M}_i}{2\pi\overline{R}\tilde{T}_s}}(\tilde{p}_i - \tilde{p}_{\mathrm{sat}}^{(i)}(\tilde{T}_s)). \tag{8}$$

Here $\tilde{T}_s$ is the surface temperature. The accommodation coefficient σ is taken to be 0.4.[18]

D. Dimensionless variables

Now we recast the main equations in terms of dimensionless variables. As a length scale, we choose the maximum bubble radius $\tilde{R}_m$. As a pressure scale, we choose the far field pressure minus the vapor pressure at $\tilde{T}_\infty$, i.e., the pressure scale is $\Delta\tilde{p} \equiv \tilde{p}_\infty - \tilde{p}_{\mathrm{sat}}(\tilde{T}_\infty)$. An associated velocity scale is $\sqrt{\Delta\tilde{p}/\tilde{\rho}_l}$. From the length scale and velocity scale, we construct the time scale $\tilde{t}_s$. The temperature scale is $\tilde{T}_\infty$. It is also convenient to define a scale for the number of moles inside the bubble, $\tilde{N}_s = \Delta\tilde{p}\tilde{R}_m^3/(\overline{R}\tilde{T}_\infty)$.

With these definitions, the evolution equation for the pressure (5) becomes

$$\frac{dp}{dt} = -\frac{\gamma p}{V}\frac{dV}{dt} + \frac{\gamma p}{N}\frac{dN}{dt} + \frac{1}{Pe_{h,g}}\frac{\gamma-1}{V}\int_{\partial V(t)} k_g \frac{\partial T_g}{\partial n}\, dA - (\gamma-1)\sum_i H_i R_i . \quad (9)$$

The evolution equation for the number of moles is

$$\frac{dN_i}{dt} = \int_{\partial V(t)} n_i v_{n,\mathrm{rel}}^{(i)} dA + R_i V. \quad (10)$$

The equation of state which determines the temperature of the interior is

$$T_g(t) = \frac{p(t)V(t)}{\Sigma_i N_i}. \quad (11)$$

The rate of evaporation or condensation of species i is

$$n_i M_i v_{n,\mathrm{rel}}^{(i)} = -\sigma \frac{1}{\sqrt{\gamma} Ma_0}\sqrt{\frac{M_i}{2\pi T_s}}\left(p_i - p_{\mathrm{sat}}^{(i)}(T_s)\right). \quad (12)$$

The balance of sensible and latent heat fluxes at the interface is

$$-k_l \frac{\partial T_l}{\partial n} = \gamma h_{lv} Pe_{h,l} Ma_0^2 \sum_i M_i n_i v_{n,\mathrm{rel}}^{(i)} h_{lv}^{(i)} - k_{r0} k_g \frac{\partial T_{g,bl}}{\partial n}. \quad (13)$$

In these equations, the dimensionless parameters are: $M_i \equiv \tilde{M}_i/\tilde{M}_0$, $R_{\mathrm{mix}} \equiv \tilde{R}_{\mathrm{mix}}/(\bar{R}/\tilde{M}_0)$, $Pe_{h,l} \equiv (\tilde{R}_m^2/\tilde{t}_s)/(\tilde{k}_{l0}/\tilde{\rho}_l \tilde{c}_{p,l})$, $Ma_l^2 \equiv (\Delta\tilde{p}/\tilde{\rho}_l)/(\tilde{c}_{p,l}\tilde{T}_\infty)$, $Ma_0^2 \equiv (\Delta\tilde{p}/\tilde{\rho}_l)/(\gamma \bar{R}\tilde{T}_\infty/\tilde{M}_0)$, $Pe_{h,g} = (Pe_{h,l} Ma_l^2)/k_{r0}$, $h_{lv} \equiv (\tilde{h}_{lv})/(\tilde{c}_{p,l}\tilde{T}_\infty)$, $k_{r0} \equiv \tilde{k}_{g0}/\tilde{k}_{l0}$, and $H_i \equiv \bar{H}_i/(\bar{R}\tilde{T}_\infty)$.

Other dimensionless parameters associated with the fluid mechanics are: the initial overpressure $\alpha = \tilde{p}_0/\Delta\tilde{p}$, the Weber number formed from the surface tension $\tilde{\sigma}_s$, and the stand-off distance $\Gamma = \tilde{z}_0/\tilde{R}_m$.

E. Slow and rapid dynamics

A basic simplification we shall exploit is to regard the dynamics at any point in time as either *slow* or *rapid*. Somewhat cruder versions of this approach (i.e., without resolution of boundary layers,[15] or with a simple model for boundary layer thickness[19,20]) were taken recently for spherical bubbles. The basic idea was found to be accurate when compared with direct numerical simulation.[15]

If the motion is slow, then the temperature and composition fields within the bubble are assumed to be uniform. During slow dynamics, water vapor freely enters or exits the bubble. Associated with evaporation or condensation, there is a small change in the interfacial temperature, but this is neglected. The temperature within the bubble is simply the far-field temperature in the liquid.

If the motion is rapid, then boundary layers form in the temperature and composition fields. The deep interior of the bubble is isolated from the liquid by a thermal and compositional boundary layer. The fraction of water vapor in the deep interior is constant, as water vapor has insufficient time to diffuse to or from the interface. The temperature in the deep interior increases or decreases owing to compression or expansion, but thermal conduction to or from the deep interior is too slow to be of direct consequence. In the compositional boundary layer, water near the interface can evaporate or condense and diffuse short distances. The rate of phase change is determined by both the temperature and the mixture composition at the interface. Hence, there is a complex coupling between phase change and the thermal boundary layers inside and outside the bubble surface.

The key innovation of our approach is to solve the convective-diffusive transport equations in the three boundary layers using a grid-free approach. This leads naturally to an integral equation statement of the balance of sensible and latent heats at the interface, which is readily solved for the interfacial temperature.

1. Slow dynamics

In the case of slow dynamics, the temperature within the bubble is uniform and sufficiently low that $R_i \approx 0$. From the equation of state, the solution to (9) should be $p(t)V(t) = N(t)$. If one substitutes this into (9) the result is

$$p\frac{dV}{dt} - \frac{dN}{dt} = \frac{1}{Pe_{h,g}}\int_{\partial V(t)} k_g \frac{\partial T_g}{\partial n}\, dA. \quad (14)$$

In other words, (14) determines the amount of heat transfer that maintains a constant bulk temperature despite a change in the volume and/or number of molecules. The number of moles changes according to

$$\frac{dN_i}{dt} = \int_{\partial V(t)} n_i v_{n,\mathrm{rel}}^{(i)} dA. \quad (15)$$

During slow dynamics, we solve (15), update the pressure using the equation of state, and determine the fluid mechanics using the boundary integral method.

2. Rapid dynamics

In the case of rapid dynamics, spatial fluxes of heat and mass relative to the mass average velocity are confined to the thermal and compositional boundary layers. In the bulk, the number of moles changes according to

$$\frac{dN_i}{dt} = R_i V. \quad (16)$$

We determine interfacial temperature from the balance of sensible and latent heats (13); the history of the interfacial temperature determines the heat and mass fluxes at the interface in a way that is developed in Sec. III. This information is used to calculate the two integrals required to update the pressure, which evolves according to

$$\frac{dp}{dt} = -\frac{\gamma p}{V}\frac{dV}{dt} + \frac{\gamma p}{N}\left[\int_{\partial V(t)} n_i v_{n,\mathrm{rel}}^{(i)} dA + R_i V\right] + \frac{1}{Pe_{h,g}}\int_{\partial V(t)} k_g \frac{\partial T_g}{\partial n}\, dA - (\gamma-1)\sum_i H_i R_i . \quad (17)$$

Hence during rapid dynamics, solution of (16) and (17) determine the number of moles in the bulk and the pressure;

next, one can update the bulk temperature from the equation of state; the interface temperature is determined using techniques developed in Sec. III; and the fluid dynamics is accounted for using the boundary integral method.

III. INTEGRAL EQUATION FOR THE BALANCE OF SENSIBLE AND LATENT HEATS AT THE INTERFACE

In this section, we develop a technique for satisfaction of the heat balance (13). This equation must be satisfied pointwise, everywhere along the interface. The strategy is as follows. The surface normal transport equations in the thermal and compositional boundary layers may be recast as canonical parabolic PDEs, for which a (convolution) integral representation of the solution may be obtained. We recast the flux terms of (13) as history integrals found by differentiating these integral representations of the solutions for the temperature and composition in the boundary layers. This constitutes an integral equation representation for (13), which is readily solved numerically for the interfacial temperature at the next time step. We begin the development with a consideration of the (convolution) integral representations of the solutions in the thermal and compositional boundary layers.

A. Thermal boundary layer outside the bubble

In this subsection, we shall develop an expression for the heat flux in the liquid at the interface, as a function of the history of the interfacial temperature. The energy equation in the liquid is, in dimensionless terms

$$\frac{\mathrm{D}T_l}{\mathrm{D}t}=\frac{1}{Pe_{h,l}}\nabla\cdot(k_l\nabla T_l). \tag{18}$$

The far-field and initial conditions are $T_l=1$.

Now we make use of the fact that surface-normal material filaments remain surface-normal at a shear-free interface. We rewrite (18) (partially) in Lagrangian coordinates (ξ,n) where at the surface, ξ is an arc length coordinate and n is a normal coordinate. The subscript 0 denotes the reference configuration. For convenience, we take this to be the time when the dynamics switches from slow to rapid. This yields

$$\left[\frac{\partial T_l}{\partial t}\right]_{\xi_0,n_0}=\frac{1}{Pe_{h,l}}\frac{1}{r}\frac{\partial}{\partial n}\left(k_l r\frac{\partial T_l}{\partial n}\right).$$

Note that the (strong) advection is accounted for by the Lagrangian coordinates; it is not neglected. One should now regard r (the distance from the axis of symmetry to the point in question) as an instantaneous function of ξ and n. Here, we are anticipating a boundary layer specialization of the energy equation in the liquid; in so doing we have neglected diffusive transport along the bubble interface in favor of diffusive transport normal to the interface. Seen in this light, the equation should now be regarded as applying to a single surface-normal material filament. Written wholly in Lagrangian terms, this equation takes the form

$$\frac{\partial T_l}{\partial t}=\frac{1}{Pe_{h,l}}\frac{1}{r}\frac{\partial n_0}{\partial n}\frac{\partial}{\partial n_0}\left(k_l r\frac{\partial n_0}{\partial n}\frac{\partial T_l}{\partial n_0}\right). \tag{19}$$

Now we pass formally to the boundary layer limit $Pe_{h,l}\to\infty$ by the introduction of the boundary layer coordinate $s\equiv -n_0 Pe_{h,l}^{1/2}\geqslant 0$. This yields the following partial differential equation along the filament:

$$\frac{\partial T_l}{\partial t}=k_l\left(\frac{\partial n_0}{\partial n}\right)^2\frac{\partial^2 T_l}{\partial s^2}. \tag{20}$$

Here the surface normal strain $\partial n_0/\partial n$ and k_l are regarded as functions of t only, if one interprets (20) as applying to a single filament at a time. Alternatively we may regard them as functions of (ξ,t) for convenience. In practice, we compute the surface normal strain from the mass (actually material volume) conservation statement $\partial n\partial A=\partial n_0\partial A_0$ where ∂A is the area of a material patch of the surface.

Now, we pursue a formal solution of (20), following the ideas of Ref. 14. We introduce a new time τ_l defined by

$$\tau_l(t)\equiv\int_0^t k_l\left(\frac{\partial n_0}{\partial n}\right)^2\mathrm{d}\hat{t}.$$

In terms of this new time, (20) becomes simply a canonical parabolic partial differential equation

$$\frac{\partial T_l}{\partial \tau_l}=\frac{\partial^2 T_l}{\partial s^2}.$$

It may be useful to consider a measure of the boundary layer thickness, which is $\delta s=\sqrt{\tau_l}$, or

$$\delta n_l=\frac{\partial n}{\partial n_0}\sqrt{\frac{\tau_l}{Pe_{h,l}}}.$$

For convenience, we transform the dependent variable to $\theta_l\equiv T_l-1$. Then the initial and far-field conditions are homogeneous. A solution may be obtained by Laplace transform, after which one computes the interfacial flux as a convolution involving the interfacial temperature:

$$\left[\frac{\partial\theta_l}{\partial s}\right]_{s=0}=\int_0^{\tau_l}\frac{1}{\sqrt{\pi(\tau_l-\phi)}}\frac{\mathrm{d}T_s}{\mathrm{d}\phi}\mathrm{d}\phi.$$

The heat flux per unit area for use in (13) is, therefore,

$$-k_l\left[\frac{\partial T_l}{\partial n}\right]_{n=0}=k_l Pe_{h,l}^{1/2}\left[\frac{\partial n_0}{\partial n}\right]_{n=0}\left[\frac{\partial\theta_l}{\partial s}\right]_{s=0}. \tag{21}$$

We note that the idea of working in a surface-normal Lagrangian coordinate appears to have been pioneered by Plesset and Zwick[21] in a spherically symmetric heat diffusion problem. Those authors used an *ad hoc* expansion technique to simplify the problem in the vicinity of the spherical surface. Thereafter, they made use of the new time τ_l to obtain the canonical parabolic partial differential equation. In Ref. 14, the same ends were accomplished in a spherical domain by use of a formal perturbation procedure, in the limit of large *Pe*. The present work is the first in which these ideas are applied in the vicinity of a nonspherical surface.

B. Thermal boundary layer inside the bubble

In this subsection, we shall develop an expression for the heat flux in the gas at the interface, as a function of the

history of the interfacial temperature and other relevant quantities. This allows for the computation of the second term on the right hand side of (13).

In order to formulate an equation for the temperature in the thermal boundary layer in the bubble interior, we begin with a dimensionless form of the energy equation equivalent to (2), but neglecting chemical reactions and terms related to the compositional diffusive flux

$$\rho c_{p,\mathrm{mix}}\frac{\mathrm{D}T}{\mathrm{D}t}-\frac{\mathrm{d}p}{\mathrm{d}t}=\frac{1}{Pe_{h,g}}\nabla\cdot(k_g\nabla T_g).$$

Because the region is cooler than the interior, these phenomena will be of lesser importance. Again we make use of the fact that surface-normal material filaments remain surface normal at a shear-free interface, but now specialized to such material filaments in the bubble interior. We rewrite this equation (partially) in Lagrangian coordinates (ξ,ν). As before, the subscript 0 denotes the reference configuration. We remark that whereas the two surface normal coordinates can be regarded as equivalent in the present configuration, $\nu=n$, this implies that $\nu_0\neq n_0$ in the past configuration owing to the fact that the gas and vapor in the interior are compressible. In the calculation, we relate ν and ν_0 via the mass conservation statement for a material volume $\rho_{gs}\partial\nu\partial A=\rho_{gs,0}\partial\nu_0\partial A_0$. Here, ρ_{gs} is the mixture density on the interface. This leads to a useful result relating the surface normal strains in the gas and liquid

$$\frac{\partial\nu}{\partial\nu_0}=\frac{\rho_{gs,0}}{\rho_{gs}}\frac{\partial n}{\partial n_0}.$$

We remark that the ratio $\rho_{gs}/\rho_{gs,0}$ varies over orders of magnitude in a strong collapse. In terms of these coordinates, we have

$$\rho c_{p,\mathrm{mix}}\left[\frac{\partial T_{g,bl}}{\partial t}\right]_{\xi_0,\nu_0}-\frac{\mathrm{d}p}{\mathrm{d}t}=\frac{1}{Pe_{h,g}}\frac{1}{r}\frac{\partial}{\partial\nu}\left(k_g r\frac{\partial T_{g,bl}}{\partial\nu}\right).$$

Note that we have written $T_{g,bl}$ to distinguish the temperature from that deep in the interior (11). As before, we have neglected diffusive transport along the bubble interface in favor of diffusive transport normal to the interface. Written wholly in terms of Lagrangian coordinates, this equation takes the form

$$\rho c_{p,\mathrm{mix}}\frac{\partial T_{g,bl}}{\partial t}-\frac{\mathrm{d}p}{\mathrm{d}t}=\frac{1}{Pe_{h,g}}\frac{1}{r}\frac{\partial\nu_0}{\partial\nu}\frac{\partial}{\partial\nu_0}\left(k_g r\frac{\partial\nu_0}{\partial\nu}\frac{\partial T_{g,bl}}{\partial\nu_0}\right). \tag{22}$$

Now we pass formally to the boundary layer limit $Pe_{h,g}\to\infty$ by the introduction of the boundary layer coordinate $\sigma\equiv\nu_0 Pe_{h,g}^{1/2}\geqslant 0$. This yields the following partial differential equation along the filament:

$$\rho c_{p,\mathrm{mix}}\frac{\partial T_{g,bl}}{\partial t}-\frac{\mathrm{d}p}{\mathrm{d}t}=k_g\left(\frac{\partial\nu_0}{\partial\nu}\right)^2\frac{\partial^2 T_{g,bl}}{\partial\sigma^2}. \tag{23}$$

The boundary and initial conditions are: $T_{g,bl}(\sigma=0,t)=T_s(t)$, $T_{g,bl}(\sigma\to\infty,t)=T_g(t)$ and $T_{g,bl}(\sigma,t=0)=1$. Note $T_s(0)=T_g(0)=1$.

Next we transform the dependent variable to $\theta_g(\sigma,t)\equiv T_{g,bl}(\sigma,t)-T_g(t)$. In terms of θ_g, the initial and far-field conditions become homogeneous. But the variable change introduces a second inhomogeneous term in the partial differential equation

$$\rho c_{p,\mathrm{mix}}\frac{\partial\theta_g}{\partial t}+\rho c_{p,\mathrm{mix}}\frac{\mathrm{d}T_g}{\partial t}-\frac{\mathrm{d}p}{\mathrm{d}t}=k_g\left(\frac{\partial\nu_0}{\partial\nu}\right)^2\frac{\partial^2\theta_g}{\partial\sigma^2}. \tag{24}$$

The two inhomogeneous terms in this equation may be neglected, for the following reason. Subject to the same assumptions as used in the derivation of the pressure evolution equation, the change in entropy of the gas mixture S is

$$\rho c_{p,\mathrm{mix}}\frac{\mathrm{d}T_g}{\partial t}-\frac{\mathrm{d}p}{\mathrm{d}t}=\frac{T_g}{V}\frac{\mathrm{d}S}{\mathrm{d}t}=\frac{1}{Pe_{h,g}}\frac{1}{V}\int_{\partial V(t)}k_g\frac{\partial T_g}{\partial n}\mathrm{d}A-\sum_i H_i R_i. \tag{25}$$

Hence, the terms involving T_g and p on the left hand side of (24) can be understood to be spatially homogeneous [see (25)]. They do not affect the flux we compute from the boundary layer solution, so we drop these terms; we are left with

$$\rho c_{p,\mathrm{mix}}\frac{\partial\theta_g}{\partial t}=k_g\left(\frac{\partial\nu_0}{\partial\nu}\right)^2\frac{\partial^2\theta_g}{\partial\sigma^2}.$$

Next, we introduce a new time τ_g defined by

$$\tau_g(t)\equiv\int_0^t\frac{k_g}{\rho c_{p,\mathrm{mix}}}\left(\frac{\partial\nu_0}{\partial\nu}\right)^2\mathrm{d}\hat{t}.$$

In terms of τ_g and σ, the PDE is transformed to the canonical parabolic equation. A measure of the boundary layer thickness is $\delta\sigma=\sqrt{\tau_g}$ or

$$\delta\nu_g=\frac{\partial\nu}{\partial\nu_0}\sqrt{\frac{\tau_g}{Pe_{h,g}}}=\frac{\partial n}{\partial n_0}\frac{\rho_{gs,0}}{\rho_{gs}}\sqrt{\frac{\tau_g}{Pe_{h,g}}}.$$

A solution for θ_g is obtained by Laplace transform, after which one computes the interfacial flux

$$\left[\frac{\partial\theta_g}{\partial\sigma}\right]_{\sigma=0}=\int_0^{\tau_g}\frac{1}{\sqrt{\pi(\tau_g-\phi)}}\frac{\mathrm{d}}{\mathrm{d}\phi}(T_s-T_g)\mathrm{d}\phi.$$

The flux for use in (13) is

$$-k_{r0}k_g\left[\frac{\partial T_{g,bl}}{\partial n}\right]_{n=0}=-k_{r0}k_g Pe_{h,g}^{1/2}\left[\frac{\partial\nu_0}{\partial\nu}\right]_{\nu=0}\left[\frac{\partial\theta_g}{\partial\sigma}\right]_{\sigma=0}. \tag{26}$$

C. Compositional boundary layer inside the bubble

Finally, we develop an expression for the vapor fraction at the interface, as a function of the history of the vapor flux due to phase change. This permits evaluation of the first term on the right hand side of (13).

In order to formulate an equation for the vapor fraction at the interface we begin with a dimensionless form of the species transport equation[16]

$$\frac{\mathrm{D}\rho_2}{\mathrm{D}t}=-\rho_2\nabla\cdot\mathbf{v}+\frac{1}{Pe_{m,g}}\nabla\cdot\left[\rho\frac{M_1M_2}{M^2}D_{21}\nabla x_2\right].$$

Here, x_2 is the mole fraction of vapor, and the Péclet number for mass transfer in the gas is $Pe_{m,g}=(\tilde{R}_m^2/\tilde{t}_s)/\tilde{D}_{21,0}$. The divergence of the mass-average velocity can be written in terms of the material derivative of ρ, which allows for the simplification to

$$\rho^2\frac{\mathrm{D}\omega_2}{\mathrm{D}t}=\frac{\rho}{Pe_{m,g}}\nabla\cdot\left[\rho\frac{M_1M_2}{M^2}D_{21}\nabla x_2\right].$$

Here ω_2 is the mass fraction of vapor. We rewrite this equation (partially) in Lagrangian coordinates $(\xi,\ \nu)$. This yields

$$\rho^2\left[\frac{\partial\omega_2}{\partial t}\right]_{\xi_0,\nu_0}=\frac{\rho}{Pe_{m,g}}\frac{1}{r}\frac{\partial}{\partial\nu}\left(\rho\frac{M_1M_2}{M^2}D_{21}r\frac{\partial x_2}{\partial\nu}\right).$$

For convenience, we write $x_2=M\rho_2/(M_2\rho)$.

As before, we have neglected diffusive transport along the bubble interface in favor of diffusive transport normal to the interface. Written wholly in terms of Lagrangian coordinates, this equation takes the form

$$\rho^2\frac{\partial\omega_2}{\partial t}=\frac{\rho}{Pe_{m,g}}\frac{1}{r}\frac{\partial\nu_0}{\partial\nu}\frac{\partial}{\partial\nu_0}\left(\rho\frac{M_1M_2}{M^2}D_{21}r\frac{\partial\nu_0}{\partial\nu}\frac{\partial x_2}{\partial\nu_0}\right).$$

Now we pass formally to the boundary layer limit $Pe_{m,g}\rightarrow\infty$ by the introduction of the boundary layer coordinate $\eta\equiv\nu_0Pe_{m,g}^{1/2}\geqslant 0$. This yields the following partial differential equation along the filament:

$$\frac{\partial\omega_2}{\partial t}=\frac{M_1}{M}D_{21}\left[\frac{\partial\nu_0}{\partial\nu}\right]^2\frac{\partial^2\omega_2}{\partial\eta^2}. \tag{27}$$

The boundary and initial conditions are: $\omega_2(\eta\rightarrow\infty,t)=\omega_{2,\infty}$, $\omega_2(\eta,t=0)=\omega_{2,\infty}$, and the flux condition at the interface

$$-\frac{\rho}{Pe_{m,g}^{1/2}}\frac{M_1}{M}D_{21}\frac{\partial\nu_0}{\partial\nu}\frac{\partial\omega_2}{\partial\eta}=M_2n_2v_{n,\mathrm{rel}}^{(2)}.$$

During rapid dynamics, $\omega_{2,\infty}$ is constant.

Next, we introduce a new time τ_c defined by

$$\tau_c(t)\equiv\int_0^t\frac{M_1}{M}D_{21}\left(\frac{\partial\nu_0}{\partial\nu}\right)^2\mathrm{d}\hat{t}.$$

In terms of τ_g and σ, the PDE is transformed to the canonical parabolic equation. The measure of the boundary layer thickness is $\delta\eta_c=\sqrt{\tau_c}$ or

$$\delta\nu_c=\frac{\partial n}{\partial n_0}\frac{\rho_{gs,0}}{\rho_{gs}}\sqrt{\frac{\tau_c}{Pe_{m,g}}}.$$

A solution is obtained by Laplace transform, after which one computes the composition at the interface as

$$\omega_2(\delta=0,\tau_c)=\omega_{2,\infty}-\frac{2}{\sqrt{\pi}}\int_0^{\tau_c}\sqrt{\tau_c-\phi}\,\frac{\mathrm{d}}{\mathrm{d}\phi}q(\phi)\mathrm{d}\phi, \tag{28}$$

where $[\partial\omega_2/\partial\eta]_{\delta=0}\equiv q$.

D. Solution method

The method is as follows. We first predict the surface velocities on the interface, and advance the interface to a predicted position. A predicted volume is computed. If the dynamics are slow, the pressure is determined once the number of moles of vapor is updated from (15). If the dynamics are rapid, the pressure is determined from (17); the number of moles in the bulk changes only by chemical reaction (16). During rapid dynamics, we predict the new interfacial temperature by iterating to satisfy (13), making use of (12), (21), (26), and (28) to write all the terms of (13) as integrals over the history of T_s. Then the time step is completed by correcting all of the values.

Finally, we describe briefly the method for switching over from slow to rapid dynamics. The idea is to make the switch when the time scale for bubble dynamics becomes shorter than the time scale for diffusive processes in the bubble interior. We must consider both diffusion of heat to the wall of the collapsing bubble, and the diffusion of vapor to the wall (where it condenses during collapse). Because the Péclet numbers for heat and mass transfer in the interior are very similar, we simply take the average of the two time scales for thermal and mass diffusion. In dimensionless terms, the dynamics is slow when

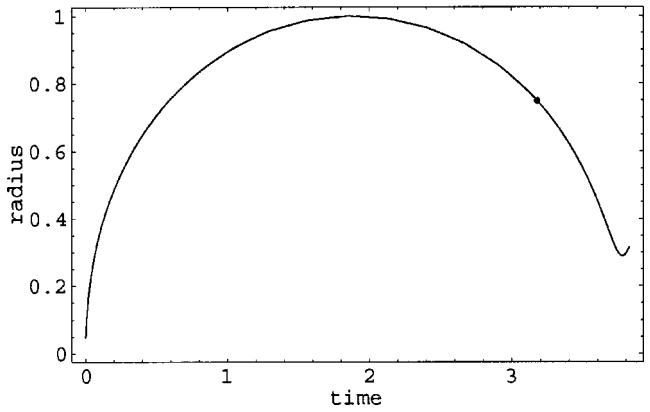

FIG. 1. Dimensionless radius of a spherical bubble versus dimensionless time. The dot shows when the dynamics switch from slow to rapid, whereupon the boundary layers commence growth. Lengths made dimensionless by $R_{\max}$.

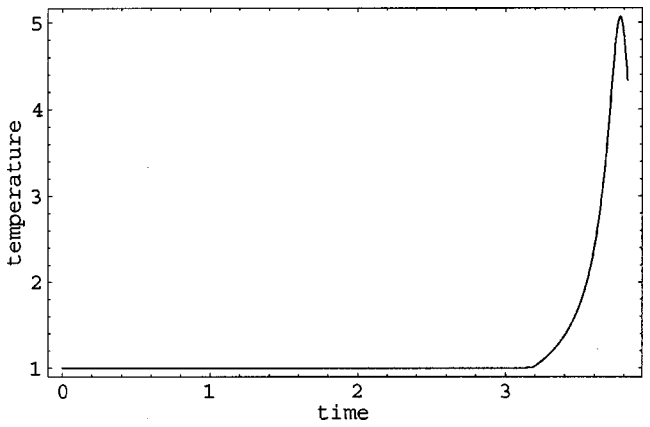

FIG. 2. Dimensionless bulk temperature versus dimensionless time for the bubble in Fig. 1.

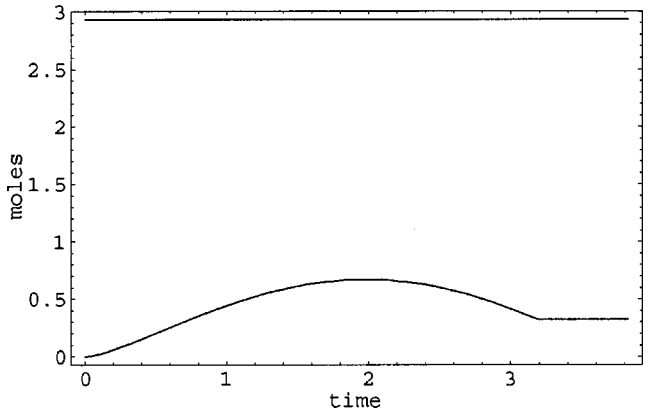

FIG. 3. Dimensionless moles of argon (upper curve) and water vapor versus dimensionless time, for the case of Fig. 1.

$$\dot{V} < 6\left(\frac{4\pi}{3}\right)^{2/3} V^{1/3}\left[\frac{D_{21}}{Pe_{m,g}} + \frac{k_g/(\rho c_{p,\mathrm{mix}})}{Pe_{h,g}}\right].$$

Otherwise it is rapid. The numerical pre-factor ensures that the bubble dynamics time scale is $R/\dot{R}$ in the special case of a spherical bubble, in agreement with our earlier work.[15]

IV. EXAMPLES

Now we turn to a demonstration of the model with several examples. To fix an example, we must define the identities of the liquid and gas; set the maximum radius, the static pressure and far-field temperature; and define the initial stand-off distance. In the present work, we consider argon bubbles in water at a static pressure of 1 bar and temperature 25 °C. The maximum radius of an equivalent isolated adiabatic bubble is set at 50 microns. The stand-off distance will be varied. The initial over-pressure is $\alpha = 1000$. The examples are not intended to be exhaustive, but rather illustrative of the kinds of results one can obtain with the model, and of the considerations that play a role in determination of the energy focusing associated with a nonspherical bubble collapse.

Although it is of interest to simulate more violent collapses than the ones we consider below, we shall here refrain from doing so for two reasons. First, more intense collapses will involve chemical changes in the gas mixture, which we neglect for simplicity in the present work. Second, laser induced cavitation bubbles, which provide a natural experimental case for comparison,[2–4,22,23] are complicated by an initial condition which it is not obvious how to model. We leave these issues for future work.

The scales and dimensionless numbers common to all the cases are as follows: length scale $\tilde{R}_m = 50\times10^{-6}$ m; time scale $\tilde{t}_s = 0.499\,261\times10^{-5}$ s; pressure scale $\Delta\tilde{p} = 100\,000.0$ Pa; temperature scale $\tilde{T}_\infty = 298.15$ K; moles scale $\tilde{N}_s = 0.504\,244\times10^{-14}$ kgmoles; liquid thermal conductivity $\tilde{k}_{l0} = 0.62$ W/m·K; gas thermal conductivity $\tilde{k}_{g0} = 0.017\,5742$ W/m·K; diffusivity of vapor in gas $\tilde{D}_{210} = 0.626\,093\times10^{-4}$ m^2/s; initial ratio of specific heats of mixture $\gamma = 1.666\,65$; Péclet number for heat transfer in the liquid $Pe_{h,l} = 3{,}365.66$; Péclet number for heat transfer in the gas $Pe_{h,g} = 9.556\,54$; Péclet number for mass transfer in the gas $Pe_{m,g} = 7.997\,85$; Mach number in the gas $Ma_0 = 0.031\,141\,6$; Mach number in the liquid Ma_l

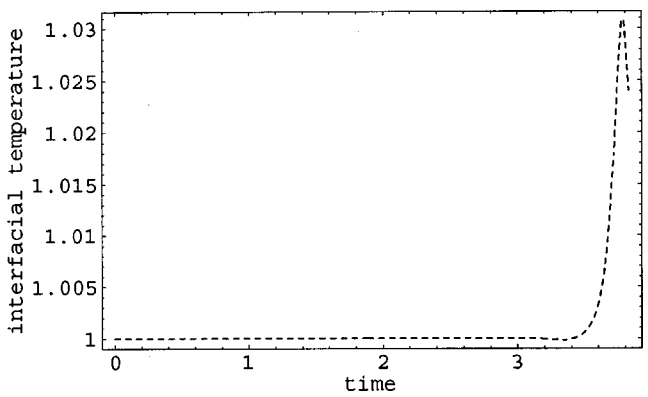

FIG. 4. Dimensionless interfacial temperature versus dimensionless time for the case of Fig. 1. For this collapse, the interface heats from 25 °C to 34.9 °C at the maximum.

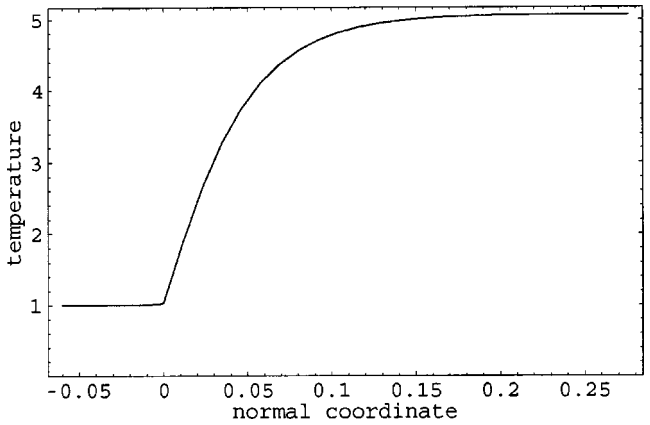

FIG. 5. Dimensionless temperature profile normal to the surface at the point of minimum volume for the bubble of Fig. 1. The location of the interface is set at 0; liquid occupies the space left of 0 and the bubble interior is to the right of 0. Lengths made dimensionless by $R_{\max}$.

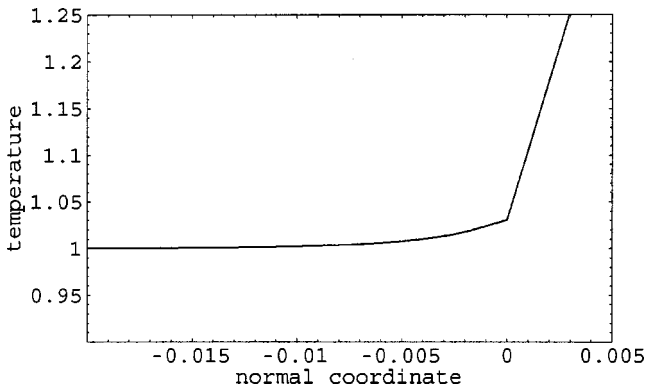

FIG. 6. Detail near the interface of the boundary layer profiles shown in Fig. 5. The kink at 0 (the interface) is a consequence of the differing thermal conductivities in the liquid (left) and gas–vapor mixture (right). Lengths made dimensionless by $R_{\max}$.

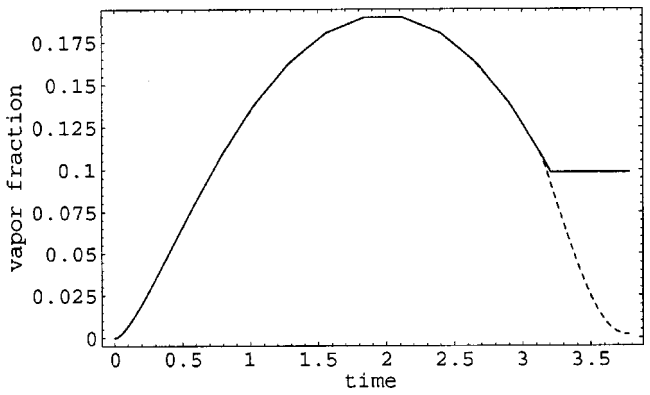

FIG. 7. Vapor fraction in the bulk (solid) and on the interface (dashed) versus dimensionless time for the case of Fig. 1.

$=0.008\,971\,32$; latent heat of vaporization $h_{lv}=1.823\,22$; Weber number $We=0.0142$. The initial radius of the bubble is $\tilde{R}_0=4.439\,294\ \mu$m.

Note that if one included heat and mass transfer, a spherical bubble subjected to these same initial conditions will grow to $\tilde{R}_{\max}=92.6789\ \mu$m rather than to the scale size $\tilde{R}_m$. For consistency with prior work in this area, we report the dimensionless stand-off distance using $\tilde{R}_{\max}$ rather than $\tilde{R}_m$.

A. Spherically symmetric bubbles

We consider first the radial case. This is achieved using the present methods by setting the dimensionless stand-off distance to be a large number and checking that no shape instability is excited during the collapse. Otherwise the spherical run we examine first is computed at the same resolution and using the same methods as the nonspherical cases we examine later.

The bubble expands as a consequence of its initial overpressure, and subsequently collapses. The *radial* response through the minimum volume is shown in Fig. 1. The dynamics switch from slow to rapid during the collapse, which traps excess heat (Fig. 2) and vapor (Fig. 3).

The compression heating of the bubble contents leads to a boundary layer between the bulk interior and the relatively cool interface. The interface heats as a result, but the relatively larger thermal capacity of the liquid limits the magnitude of this increase (Fig. 4). The conduction of heat to the interface from the interior leads to a thinner boundary layer in the liquid outside the bubble. These thermal boundary layers are depicted in Fig. 5 and in a close view in Fig. 6. The profiles in Figs. 5 and 6 are reconstructed from the solutions of the thermal transport equations. This is done only for the purposes of visualization; it is never necessary to determine the whole boundary layer profile to compute T_s by the methods we have described above.

Of great importance to the determination of the interfacial temperature is the concentration boundary layer, which results from the diffusion of vapor from the bulk to the interface. During rapid dynamics, the interfacial vapor fraction drops far below the bulk vapor fraction (Fig. 7), just as the interfacial temperature is much less than the bulk temperature.

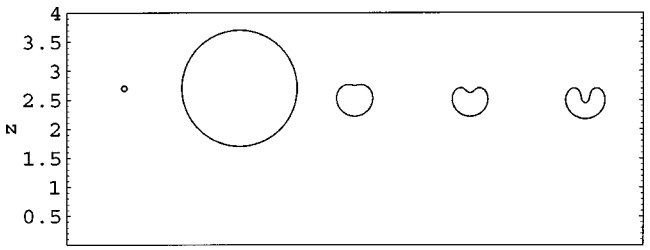

FIG. 8. Snapshots of the shape and position of a bubble growing and collapsing near a solid wall or another bubble. The dimensionless times are 0, 2.115 54 (time of maximum volume), 4.014 09, 4.063 74 (time of minimum volume), and 4.157 42, plotted left to right. The dimensionless stand-off distance is $z_0/R_{\max}=2.697\,48$. Lengths made dimensionless by $R_{\max}$.

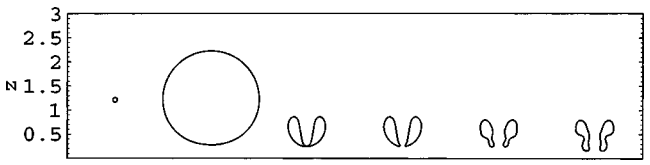

FIG. 9. Snapshots of the shape and position of a bubble growing and collapsing near a solid wall or another bubble. The dimensionless times are 0, 2.065 96 (time of maximum volume), 4.300 01 (time just before toroidal transition), 4.300 10 (time just after toroidal transition), 4.368 25 (time of minimum volume), 4.413 01, plotted left to right. The dimensionless stand-off distance $z_0/R_{\max}=1.213\,87$. Lengths made dimensionless by $R_{\max}$.

B. Nonspherical bubbles

Now we consider the same size and initial composition of bubble, with the same initial overpressure, but now near a solid wall—or twice the distance from a bubble of identical size. The calculations of the fluid mechanics exploit the boundary integral method and code of Blake *et al.*[8–10] and later development by Pearson *et al.*[24] An example of such a

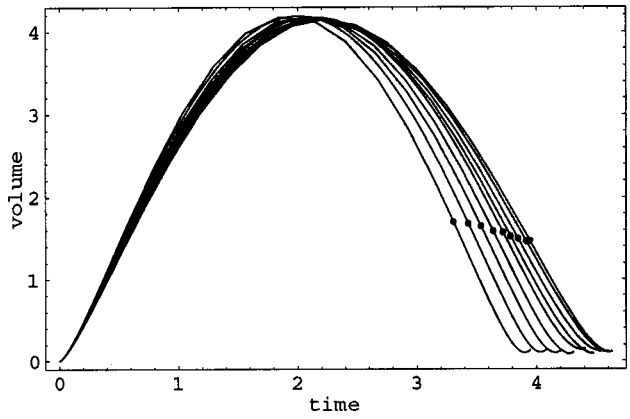

FIG. 10. Dimensionless volume of nonspherical bubbles versus dimensionless time. The dots indicate the point in time where the dynamics switch from slow to rapid. Collapses nearer the wall are delayed longer. The dimensionless stand-off distance of the runs shown is $z_0/R_{\max}=5.394\,97$, 2.697 48, 1.888 24, 1.483 62, 1.213 87, 1.078 99, 0.944 119, 0.809 245, and 0.728 32 from left to right. The bubbles have the same contents at time $t=0$, and are driven by the same pressure difference. Lengths made dimensionless by $R_{\max}$.

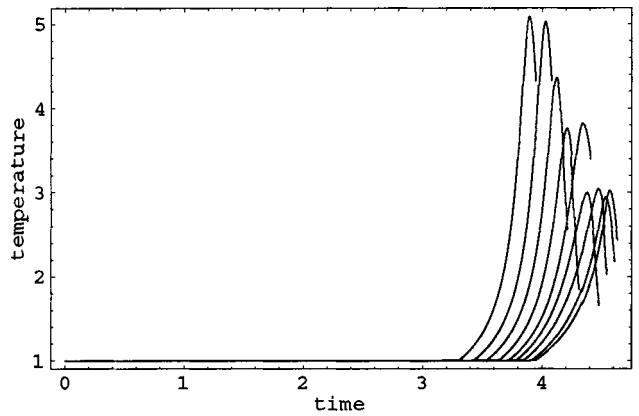

FIG. 11. Dimensionless bulk temperature versus dimensionless time for the nonspherical bubbles in Fig. 10. The bulk temperature curves depart from 1 in descending order with the stand-off distance. Bubbles nearer the wall have lower peak temperatures, generally, but there is no monotonic relationship owing to a sensitive dependence of the minimum volume at collapse on the details of the bubble shape, as shown in Fig. 12.

collapse, which leads to an inwardly directed jet that does not, however, traverse the interior to the other side before the bubble reaches minimum volume, is shown in Fig. 8. A second example in Fig. 9 shows a topological transition to a toroidal bubble.

For otherwise initially identical bubbles at varying stand-off distance, we show the dimensionless volumes (Fig. 10) and bulk temperatures (Fig. 11) versus time. Collapses of more closely spaced bubbles are delayed relative to more distantly spaced bubbles. Those which are close enough undergo transition to a toroidal geometry, whereupon the collapse continues until the minimum toroidal volume is reached before re-expansion. The volume minima of bubbles nearer the wall, which are toroidal, are more gradual; the corresponding temperature peaks are generally considerably lower than unconstrained bubbles at large stand-off. However, the peak temperatures are a sensitive function of the shape and volume at minimum volume, which varies considerably with stand-off distance (Fig. 12).

In the final analysis, the importance of modeling heat and mass transfer is to enable accurate prediction of peak temperatures in the bubble interior at a violent nonspherical collapse. This may be appreciated from the following comparison. We compare the case of a bubble growth and collapse computed with full heat and mass transfer (using the

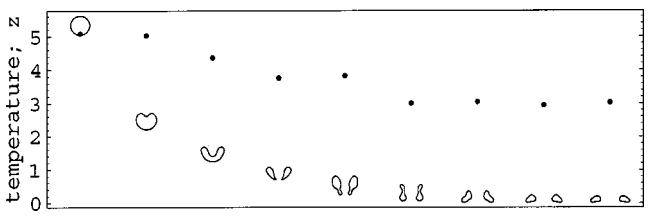

FIG. 12. Shape at minimum volume and dimensionless peak temperature for the bubbles of Fig. 10. The shapes are shown with the actual stand-off distance at minimum volume, for bubbles initiated at decreasing stand-off distance from left to right. Note that in some cases the minimum volume occurs for simply connected bubbles; in other cases the volume minimum is achieved by toroidal bubbles. Lengths made dimensionless by R_{max}.

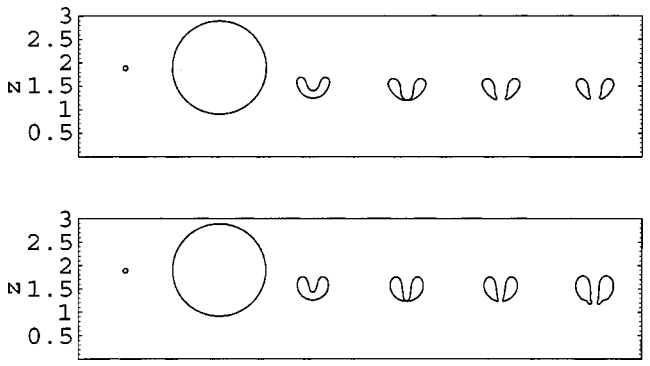

FIG. 13. Shapes at equivalent times for comparable bubbles, except that the upper row is computed with full heat and mass transfer, and the lower row is computed for the gross approximation of no mass transfer, and isothermal to adiabatic switching at the slow to rapid transition time. The snapshots are at the following times: Initial condition (upper time 0, lower 0), maximum volume (2.102 68, 2.014 54), minimum volume (4.155 69, 4.049 01), before toroidal transition (4.212 77, 4.089 03), after toroidal transition (4.212 79, 4.089 09), final (4.213 33, 4.139 05). The dimensionless stand-off distance of the runs shown is $z_0/R_{max}=1.88824$. Lengths made dimensionless by R_{max} for the case with full heat and mass transfer.

methods of the present work) with that based on a much simpler approximation. In the simpler approximation, when the dynamics are slow, the bubble is treated as an isothermal constant mass system. When the dynamics are rapid, the bubble is treated as an adiabatic system. This approximation leads to more physically accurate results than a simple constant polytropic approximation, which suffers from intense and unrealistic expansion cooling owing to the suppression of evaporation. The comparison is shown in Figs. 13–15. The isothermal-adiabatic bubble grows to a smaller maximum radius, collapses earlier, but with a significantly higher peak temperature than the model of the present work. The smaller maximum radius and earlier collapse are associated with suppression of influx of vapor. The higher peak temperature of the isothermal-adiabatic bubble is associated with the adiabatic collapse, during which no energy is lost to the liquid.

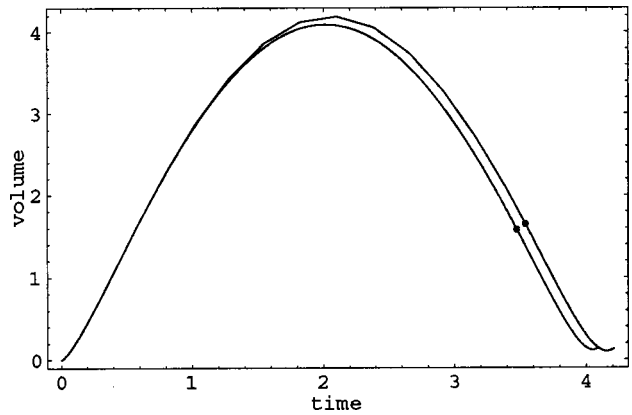

FIG. 14. Dimensionless volume versus dimensionless time for the two comparable bubbles of Fig. 13. The bubble with full heat and mass transfer grows larger and collapses later. Lengths made dimensionless by R_{max} for the case with full heat and mass transfer.

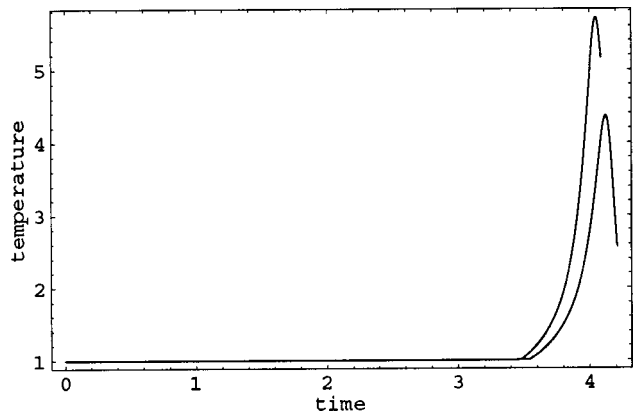

FIG. 15. Dimensionless bulk temperature versus dimensionless time for the two comparable bubbles of Fig. 13. The bubble with the gross approximation of no mass transfer, and isothermal to adiabatic switching at the slow to rapid transition time has a higher peak temperature than the one computed with full heat and mass transfer.

V. CONCLUSIONS

Bubbles may collapse with such violence that the relatively slow processes of diffusion of the heat of compression and of excess vapor to the bubble wall are nearly obviated. This leads to an approximately adiabatic system with nearly constant mass during the final stages of extreme collapses, accompanied by the evolution of sharp thermal and compositional boundary layers on either side of the interface. We have shown in the present work that the boundary layers, which are involved in the determination of the interfacial temperature through the balance of sensible and latent heats, may profitably be described mathematically through integral equations. This complements well the boundary integral solution of the fluid dynamics, which has been the basis of much progress in the field.

The numerical technique has been applied to a number of different collapses of bubbles either isolated or in close proximity to a like bubble or a wall. The peak temperature reached during the collapse is generally lower for bubbles near a neighbor or wall than for bubbles isolated in space. However, the inefficiency of nonspherical relative to spherical collapse is a sensitive function of the proximity of the neighboring bubble or wall.

ACKNOWLEDGMENTS

A.J.S. would like to acknowledge support from the National Science Foundation Program in Theoretical Physics and a Research Fellowship from the Alexander von Humboldt Foundation; he would also like to thank Professor Dr. W. Lauterborn for hosting a pleasant stay in Göttingen. A.P. acknowledges support from EPSRC. A.J.S. is also grateful to Dr. Olgert Lindau for useful discussions.

[1] J. R. Blake and D. C. Gibson, "Cavitation bubbles near boundaries," Annu. Rev. Fluid Mech. **19**, 99 (1987).
[2] A. Vogel, W. Lauterborn, and R. Timm, "Optical and acoustic investigations of laser-produced cavitation bubbles near a solid boundary," J. Fluid Mech. **206**, 299 (1989).
[3] C.-D. Ohl, O. Lindau, and W. Lauterborn, "Luminescence from spherically and aspherically collapsing laser induced bubbles," Phys. Rev. Lett. **80**, 393 (1998).
[4] C.-D. Ohl, "Probing luminescence from nonspherical bubble collapse," Phys. Fluids **14**, 2700 (2002).
[5] H. Yuan and A. Prosperetti, "Gas–liquid heat transfer in a bubble collapsing near a wall," Phys. Fluids **9**, 127 (1997).
[6] A. Yasuda and H. Takahira, "Numerical analysis of temperature fields inside nonspherical bubbles in the final stages of collapse," Proceedings of the Fourth International Symposium on Cavitation, Pasadena, 2001; H. Takahira, A. Yasuda, and A. Uemura, "Effects of heat transfer of internal gas on bubble collapse near a compliant wall," Proceedings of the 5th JSME-KSME Fluids Engineering Conference, Nagoya, 2002.
[7] B. B. Taib, "Boundary integral method applied to cavitation bubble dynamics," Ph.D. dissertation, University of Wollongong, Department of Mathematics, 1985.
[8] J. R. Blake, B. B. Taib, and G. Doherty, "Transient cavities near boundaries. Part 1. Rigid boundary," J. Fluid Mech. **170**, 479 (1986).
[9] J. R. Blake, M. C. Hooton, P. B. Robinson, and R. P. Tong, "Collapsing cavities, toroidal bubbles, and jet impact," Philos. Trans. R. Soc. London, Ser. A **355**, 537 (1997).
[10] J. R. Blake, G. S. Keen, R. P. Tong, and M. Wilson, "Acoustic cavitation: The fluid dynamics of nonspherical bubbles," Philos. Trans. R. Soc. London, Ser. A **357**, 251 (1999).
[11] G. K. Batchelor, *An Introduction to Fluid Dynamics* (Cambridge University Press, Cambridge, 2000).
[12] J. M. Boulton-Stone, "The effect of surfactant on bursting gas bubbles," J. Fluid Mech. **302**, 231 (1995).
[13] J. M. Boulton-Stone and J. R. Blake, "Gas bubbles bursting at a free surface," J. Fluid Mech. **254**, 437 (1993).
[14] M. M. Fyrillas and A. J. Szeri, "Dissolution or growth of soluble, spherical, oscillating bubbles," J. Fluid Mech. **277**, 381 (1994).
[15] B. D. Storey and A. J. Szeri, "A reduced model of cavitation physics for use in sonochemistry," Proc. R. Soc. London, Ser. A **457**, 1685 (2001).
[16] R. B. Bird, W. E. Stewart, and E. N. Lightfoot, *Transport Phenomena* (Wiley, New York, 1960).
[17] V. P. Carey, *Liquid–Vapor Phase Change Phenomena* (Taylor & Francis, London, 1992).
[18] B. D. Storey and A. J. Szeri, "Water vapor, sonoluminescence and sonochemistry," Proc. R. Soc. London, Ser. A **456**, 1685 (2000).
[19] R. Toegel, B. Gompf, R. Pecha, and D. Lohse, "Does water vapor prevent up-scaling sonoluminescence?" Phys. Rev. Lett. **85**, 3165 (2000).
[20] T. J. Matula, P. R. Hilmo, B. D. Storey, and A. J. Szeri, "Radial response of individual bubbles subjected to shock wave lithotripsy pulses *in vitro*," Phys. Fluids **14**, 913 (2002).
[21] M. S. Plesset and S. A. Zwick, "A nonsteady heat diffusion problem with spherical symmetry," J. Appl. Phys. **23**, 95 (1952).
[22] C.-D. Ohl, T. Kurz, R. Geisler, O. Lindau, and W. Lauterborn, "Bubble dynamics, shock waves and sonoluminescence," Philos. Trans. R. Soc. London, Ser. A **357**, 269 (1999).
[23] O. Baghdassarian, B. Tabbert, and G. A. Williams, "Luminescence from laser-created bubbles in cryogenic liquids," Physica B **284**, 393 (2000).
[24] A. Pearson, J. R. Blake, and S. R. Otto, "Jets in bubbles," J. Eng. Math. (to be published).